Laboratory studies of magnetic vortices. III. Collisions of electron magnetohydrodynamic vortices

J. M. Urrutia, R. L. Stenzel, and M. C. Griskey
Department of Physics and Astronomy, University of California, Los Angeles, California 90095-1547

(Received 22 March 1999; accepted 18 October 1999)

Magnetic vortices in the parameter regime of electron magnetohydrodynamics are studied in a large laboratory plasma. The vortices consist of magnetic field perturbations, which propagate in the whistler mode along a uniform dc magnetic field. The magnetic self-helicity of the spheromak-like field perturbations depends on the direction of propagation. Vortices with opposite toroidal or poloidal fields are launched from two antennas and propagated through each other. The vortices collide and propagate through one another without an exchange of momentum, energy, and helicity. The absence of nonlinear interactions is explained by the force-free fields of electron magnetohydrodynamic (EMHD) vortices. © *2000 American Institute of Physics.* [S1070-664X(00)01202-7]

I. INTRODUCTION

Electron magnetohydrodynamics (EMHD) describes the plasma parameter regime where electrons are fully magnetized while ions are essentially unmagnetized.[1] Typically, this holds in the frequency regime $\omega_{ci} \ll \omega \ll \omega_{ce}$, where ω_{ci}, ω_{ce} are the ion and electron cyclotron frequencies, respectively, and on spatial scale lengths between the electron and ion inertial scale lengths, $c/\omega_{pe} < L < c/\omega_{pi}$, where ω_{pi}, ω_{pe} are the ion and electron plasma frequencies, respectively. The different response of the electron and ion fluids produces phenomena not present in single-fluid MHD: Ohm's law is dominated by the Hall effect, magnetic fields are frozen into the electrons and transported by electron whistler waves, and field topologies are always three dimensional (3-D) and exhibit helicity. These conditions arise in many natural and manmade plasmas. In space, reconnection at magnetic null points involves a transition from MHD to EMHD physics because, as $B \to 0$, the ions become unmagnetized before the electrons.[2,3] Magnetic fluctuations in the solar wind beyond the MHD dissipation range also involve EMHD effects.[4,5] In laboratory plasmas, EMHD governs the physics of helicon plasma sources,[6] plasma opening switches,[7] rotamak fusion devices,[8] and basic plasma experiments on transient currents.[9,10] The latter demonstrated the existence of 3-D EMHD vortices, as suggested by earlier theories.[11] These vortices are spheromak-like magnetic field perturbations, which propagate in the whistler mode along a uniform background magnetic field. They have many interesting properties: The linked toroidal and poloidal fields exhibit helicity whose sign is uniquely related to the direction of propagation along $\mathbf{B}_0$. The perturbed vector potential $\mathbf{A}$, magnetic field $\mathbf{B} = \nabla \times \mathbf{A}$, current density $\mathbf{J} = \nabla \times \mathbf{B}/\mu_0$, and electron vorticity $\omega_e = \nabla \times \mathbf{v}_e = -\nabla \times \mathbf{J}/ne$ are approximately all aligned. The vortices are force-free structures satisfying $\mathbf{J} \times \mathbf{B}_{\text{tot}} - ne\mathbf{E} \simeq 0$ in a uniform plasma. Because in EMHD the electric and magnetic forces on the electron fluid essentially cancel, two parallel currents do *not* cause the electron fluid to attract. This behavior is fundamentally different from MHD plasmas or conductors in free space, where the $\mathbf{J} \times \mathbf{B}$ force dominates. Indeed, observations confirm that in EMHD a cylindrical current does not easily pinch[12] or a current sheet does not readily tear.[13] Similarly, EMHD waves (whistler vortices) remain linear up to relatively large amplitudes ($B_{\text{wave}} \leqslant B_0$) or energy densities ($B_{\text{wave}}/2\mu_0 > nkT_e$), which is neither the case for MHD waves or electrostatic waves. These properties are thought to explain why EMHD vortices do not interact as nonlinearly as vortices in fluid and gasdynamics,[14] non-neutral plasmas,[15] and the formation of MHD turbulence.[16,17]

In the present work we deal with collisions of 3-D vortices in an electron fluid. In contrast to other fluids, the interaction is found to be entirely linear, i.e., the vortices propagate through each other without exchange of energy or momentum. The combined field is a linear superposition of the fields of the individual pulses, both for head-on and glancing collisions. This apparently simple result is surprising since earlier observations on the interaction of MHD plasmoids with force-free fields showed billiard-ball-like collisions.[18] It is explained by the balance of magnetic and electric forces in EMHD fields.

The paper is organized as follows: After describing in Sec. II the plasma device and measurement techniques, the experimental results are presented in Sec. III, divided into various subsections. In the conclusion, Sec. IV, we point out the relevance of the present findings to related observations and applications.

II. EXPERIMENTAL ARRANGEMENT

The experiments are performed in a large laboratory plasma device schematically shown in Fig. 1. A 1 m diam×2.5 m long plasma column of density $n_e \simeq 6 \times 10^{11}\,\text{cm}^{-3}$ and electron temperature $kT_e \simeq 1.5\,\text{eV}$ ($p_n \simeq 0.26\,\text{mTorr, Ar}$), is produced in a uniform axial magnetic field $B_0 \simeq 5-10\,\text{G}$ with a pulsed dc discharge ($V_{\text{dis}} \simeq 50\,\text{V}$, $I_{\text{dis}} \simeq 600\,\text{A}$, $t_{\text{pulse}} \simeq 5\,\text{ms}$, $t_{\text{rep}} \simeq 1\,\text{s}$) using a large oxide-coated cathode.[19] In the quiescent, uniform, current-free afterglow

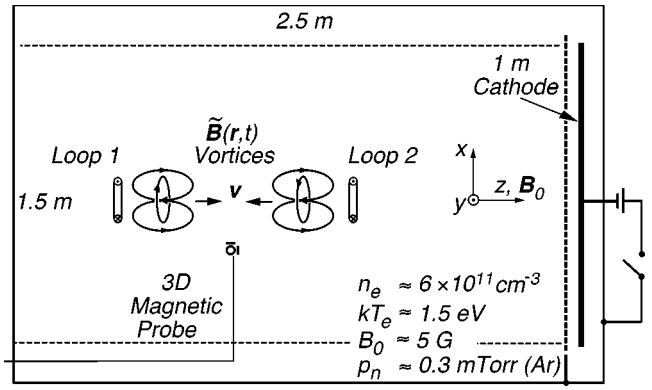

FIG. 1. Experimental setup and basic plasma parameters.

plasma, pulsed currents are applied to two identical magnetic loop antennas ($\sim$10 cm diam, 1 turn) separated axially by $\Delta z = 50$ cm. The time-varying magnetic fields associated with the plasma currents are measured with a triple magnetic probe, recording (B_x, B_y, B_z) versus time at a given position. By repeating the highly reproducible discharges and moving the probe to many positions in a volume, the vector field $\mathbf{B}(\mathbf{r},t)$ is obtained with high resolution ($\Delta r \simeq 1$ cm, $\Delta t \simeq 10$ ns). The spatial field distribution at any instant of time can be constructed from the digitally stored temporal traces. Plasma parameters are obtained from a small Langmuir probe ($\pi r^2 \simeq 2.6\,\mathrm{mm}^2$) which is also movable in three dimensions.

III. EXPERIMENTAL RESULTS

A. Excitation of whistler vortices from a loop antenna

We start with a brief review of the penetration of transient magnetic fields into a uniform magnetoplasma. Combining Faraday's law and the force-free condition in an ideal plasma yields $\partial\mathbf{B}/\partial t = \nabla\times(\mathbf{v}\times\mathbf{B})$. The equation describes magnetic fields frozen into the fluid of velocity $\mathbf{v}$, which, in EMHD,[1] is the electron fluid velocity, $\mathbf{v}_e = -\mathbf{J}/ne = -\nabla\times\mathbf{B}/ne\mu_0$. For small field perturbations $[B(\mathbf{r},t) \ll B_0]$, propagating with wave velocity $v_\parallel = \pm\partial z/\partial t$ along the dc magnetic field $\mathbf{B}_0$, the linearized solution of $\partial\mathbf{B}/\partial t = -\nabla\times(\mathbf{J}\times\mathbf{B})/ne$ yields $\mathbf{J}/ne = \pm v_\parallel\mathbf{B}/B_0$. Here, the wave velocity is that of low-frequency whistlers since Fourier transformation of the differential equation yields the whistler dispersion relation, $\omega = k^2(B_0/ne\mu_0) = (kc/\omega_{pe})^2\omega_{ce}$. Bounded wave packets consisting of a spectrum ($\Delta\mathbf{k}$, $\Delta\omega$) of oblique whistlers can form 3-D vortices[11] consisting of linked toroidal and poloidal fields like those in a Hill's vortex[20] or a spheromak.[21] Vortices with $\mathbf{J} \parallel \pm\mathbf{B} \parallel \pm\mathbf{A}$ have positive helicity densities for propagation along the dc magnetic field $\mathbf{B}_0$ and negative helicities for propagation opposite to $\mathbf{B}_0$. The total magnetic helicity, an invariant in ideal fluids, can be decomposed into mutual and self-helicities, $H_{\mathrm{tot}} = H_{\mathrm{self}} + H_{\mathrm{mutual}} = \int(\mathbf{A}_0+\mathbf{A})\cdot(\mathbf{B}_0+\mathbf{B})\,dV = \int\mathbf{A}\cdot\mathbf{B}\,dV + \int\mathbf{A}_0\cdot\mathbf{B}\,dV$, the first term describing the topology of the perturbed field $\mathbf{B}(\mathbf{r},t)$, and the second the linkage of $\mathbf{B}(\mathbf{r},t)$ with $\mathbf{B}_0$. For small perturbations the vortex topology exists only in the perturbed magnetic field and the electron fluid velocity. The total magnetic field lines exhibit a propagating twist and bulge or pinch depending on vortex polarity. However, if the vortex field exceeds the ambient field magnetic null points or lines can be formed.

Fourier analysis of the experimental data[22] reveals that the electromagnetic perturbation consists of oblique whistler modes, which form 3-D vortices, as predicted by theory.[11] Physically, the spheromak-like vortex can be thought of as produced by the linkage between a toroidal field B_θ formed by axial currents, and an axially oriented poloidal (dipolar) field (B_r, B_z) formed by toroidal Hall currents. The currents are driven by both inductive and space-charge electric fields.[10,22] Vortices are excited by pulsed currents applied to a simple loop antenna with its dipole axis along a uniform dc magnetic field $\mathbf{B}_0$. A current step excites one vortex in time, a current pulse excites a sequence of two vortices of opposite polarity, an ac current produces oscillating vortices. The poloidal or dipolar vortex field is induced by a loop antenna. The toroidal field develops self-consistently, as follows:[23] The toroidal inductive electric field $(E_\theta \propto \partial B_z/\partial t)$ gives rise to a radial electron drift, $v_r \simeq E_\theta/B_0$. Since the electrons are essentially incompressible ($\nabla\cdot\mathbf{J} \simeq 0$), the diverging radial current is closed by axial currents $\pm J_z$ driven by a parallel electric field due to a small space-charge imbalance ($n_i - n_e \gg n_i$) at the center of the antenna/vortex. Radial and axial currents form a poloidal current loop. The axial currents produce toroidal fields $\pm B_\theta$, which link the poloidal field (B_r, B_z) to form two vortices propagating in opposite directions with opposite helicity. In the propagating vortices, the poloidal field is generated by toroidal Hall currents $J_\theta \simeq neE_r/B_0$ associated with the space-charge imbalance inside the vortex. In the absence of collisions the adiabatic compression/expansion of electrons does not create energy losses or net electron heating.

Figure 2 presents a measurement example of such vortex properties. Figure 2(a) shows a snapshot of the toroidal field components (B_x, B_y) in an $x-y$ plane in the middle of the vortex, while Fig. 2(b) shows the poloidal field (B_y, B_z) in an $x-z$ plane on axis. The poloidal vector field is enhanced by tracing a few field lines that clarify the right-handed linkage between the toroidal and poloidal field components. The magnetic self-helicity is positive for wave propagation along $\mathbf{B}_0$. The V-shaped poloidal field arises from the fact that oblique whistler modes propagate slower than parallel whistlers inside the slowly expanding vortex.

B. Head-on collisions of vortices

Two identical loop antennas with dipole moments $\mathbf{m} \parallel \mathbf{B}_0$ are placed on the axis ($x = y = 0$) and separated by $\Delta z = 50$ cm, as schematically shown in Fig. 1. When energized by the same current pulses, two vortices of identical poloidal but opposite toroidal fields propagate against one another [Fig. 3(a)]. When the currents in the two antennas flow in opposite directions, two vortices with opposite poloidal and identical toroidal fields are made to collide [Fig. 3(b)]. As the two vortices of opposite helicity collide, the opposing field components are expected to cancel while the identical fields add, leaving either a purely poloidal field

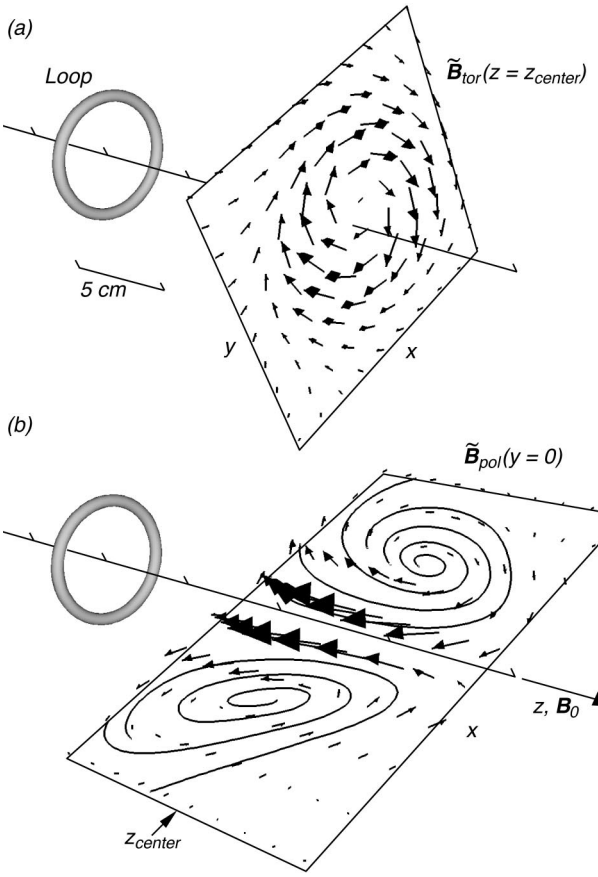

FIG. 2. Topology of a magnetic vortex in the perturbed magnetic field $\tilde{\mathbf{B}}(\mathbf{r},t)$ propagating in the whistler mode along a uniform field $\mathbf{B}_0$. (a) Vector field of the toroidal field component in the transverse $x-y$ plane in the center of the vortex. (b) Poloidal field ($\tilde{B}_x$, $\tilde{B}_z$) in an $x-z$ plane at $y=0$. It is produced by a toroidal current induced by the exciter loop antenna. For propagation along $\mathbf{B}_0$ the vortex fields have right-handed linkage or positive magnetic self-helicity.

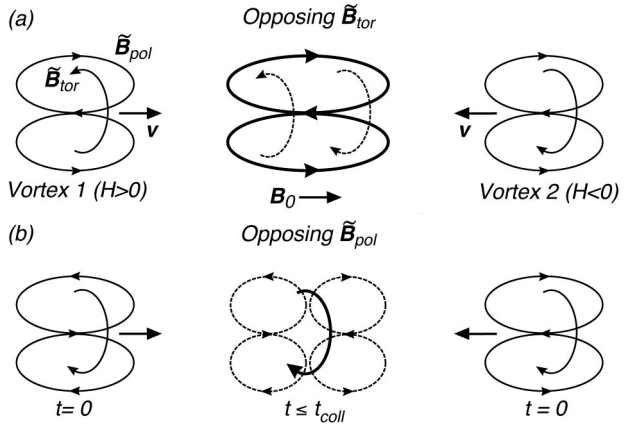

FIG. 3. Schematic figure explaining the expected fields during the head-on collision of vortices of opposite helicity. Either toroidal (a) or poloidal fields (b) may cancel during the collision.

[Fig. 3(a)] or a purely toroidal field [Fig. 3(b)] at the moment of collision. In the former case, a toroidal null line is formed at the midplane between the antennas; in the latter, a cusp-type null point is generated. Total zero helicity is conserved at all times.

Experimental observations corresponding to Fig. 3(a) have been performed for two cases: (i) a small-amplitude single vortex generated by a fast-rising ($t_{\text{rise}} \simeq 100$ ns) current step (7 A), and (ii) a large-amplitude vortex ($B_{z,\max} \leqslant B_0$) generated by a stronger (85 A) but slower ($t_{\text{pulse}} \simeq 5\ \mu$s) current pulse through the antenna. For the small-amplitude vortex ($B_{\max}/B_0 < 1\%$), Fig. 4 displays contours of the toroidal field B_θ ($=B_x$ for $x=0$, $y<0$) versus axial position z and time t for each vortex separately (first two frames), for both vortices together (third frame), and for the linear superposition of the two individual vortices (fourth frame), i.e., the additions of the first two frames in Fig. 4. Dashed lines along the crests indicate the vortex propagation at the whistler speed ($v_\parallel \simeq \pm 8.8 \times 10^7$ cm/s). The third and fourth frames of Fig. 4 are identical to within experimental accuracy. In the symmetry plane ($z=0$), the opposing fields $\pm B_\theta$ cancel at all times during the penetration of the oppositely propagating vortices. At the time of collision ($t \simeq 0.4\ \mu$s), the toroidal field vanishes at all axial positions, i.e., it is completely annihilated. After the collision, both vortices continue to travel in opposite directions with amplitudes and velocities comparable to those of the individual vortices. Thus, the collision has caused no change in momentum, energy, or magnetic helicity. These results may not be surprising since the wave field is very small compared to the ambient field and the wave energy density is small compared to the particle energy density.

Figures 5 and 6 display field components for the large-amplitude case, where the applied antenna field exceeds the ambient field ($B_{\text{ant,max}} \simeq 2B_0$). Since we are interested in the collision of the vortices, the vacuum field of the dipole has been subtracted from the time-dependent field in the plasma (B_0 not included). However, due to coupling losses, wave spread, and damping, the ratio of the actual fields, $B_{\text{pl,max}}/B_0$, during collision is about 20%. Nevertheless, electrostatic waves of comparable normalized wave densities would produce strong nonlinearities, as evidenced in soliton collisions.[24–26] The observed toroidal field components B_θ (Fig. 5) and poloidal field components B_z (Fig. 6) are displayed in $y-z$ planes ($x=0$) for four cases, i.e., each vortex propagating separately, both vortices launched together, and a linear superposition of the two individual vortices. The data are shown prior to ($t=1.25\ \mu$s), during ($t=2.15\ \mu$s), and after the collision ($t=3.75\ \mu$s). As expected, the toroidal fields cancel and the poloidal (axial) fields add during the collision. The observations show that even for these large-amplitude vortices there is no significant differences between the actual fields of the two colliding vortices and the linear superposition of the two individual vortices propagating in opposite directions. Thus, force-free vortices do not interact with one another.

Figure 7 supports the same conclusions from complementary field measurements in the transverse $x-y$ plane where the collision occurs ($z=0$). The toroidal fields (B_x, B_y) $\simeq B_\theta$ are shown as vector fields at the top, the poloidal fields B_z as contour plots at the bottom at the time of collision ($t=2.15\ \mu$s) for the same four cases as in Figs. 5 and 6. The poloidal fields B_z of the two vortices add during

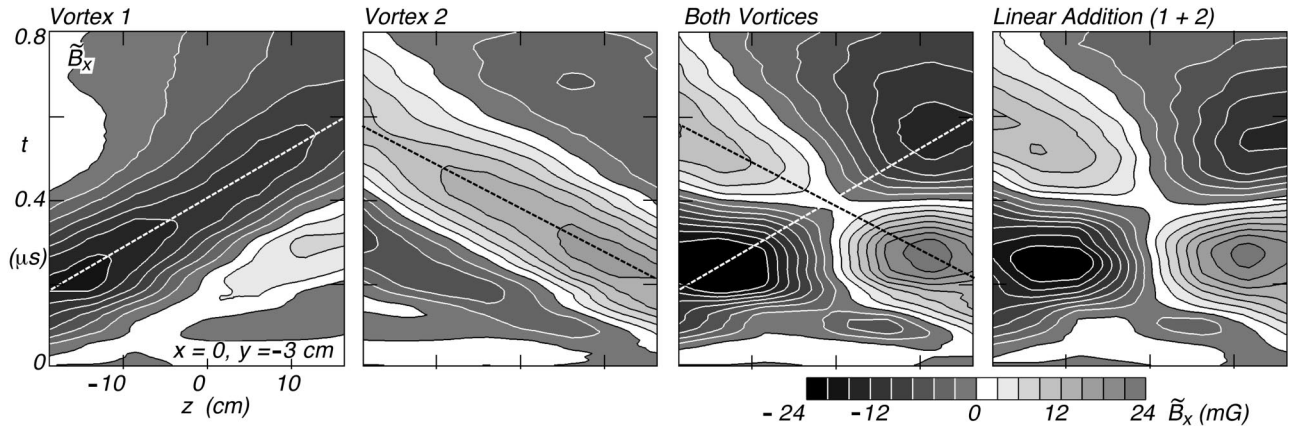

FIG. 4. Toroidal field component $\tilde{B}_\theta$ versus axial position z ($x=0$, $y=-3$ cm) and time t for the head-on collision of small-amplitude vortices with opposing $\tilde{B}_\theta$ ($B_0=10$ G). Four cases are shown horizontally, i.e., each vortex propagating separately, both together, and a linear superposition of the two individual vortices. The vortices propagate through one another without nonlinear interactions.

the collision, while the toroidal fields B_θ nearly cancel, the difference arising from a small offset in the vertical antenna alignment. Zero helicity is conserved, the ''loss'' of toroidal field energy is balanced by the gain in poloidal energy. Energy is conserved in the interaction since after the collision the vortices emerge with the same fields as noncolliding vortices.

During the propagation and collision of the two vortices the net magnetic field lines behave as schematically shown in Fig. 8. The vortices create an azimuthal twist and radial pinch, which, for the purpose of clarity, are discussed separately but occur together. Figure 8(a) shows the azimuthal displacement of a typical off-axial field line due to the op-

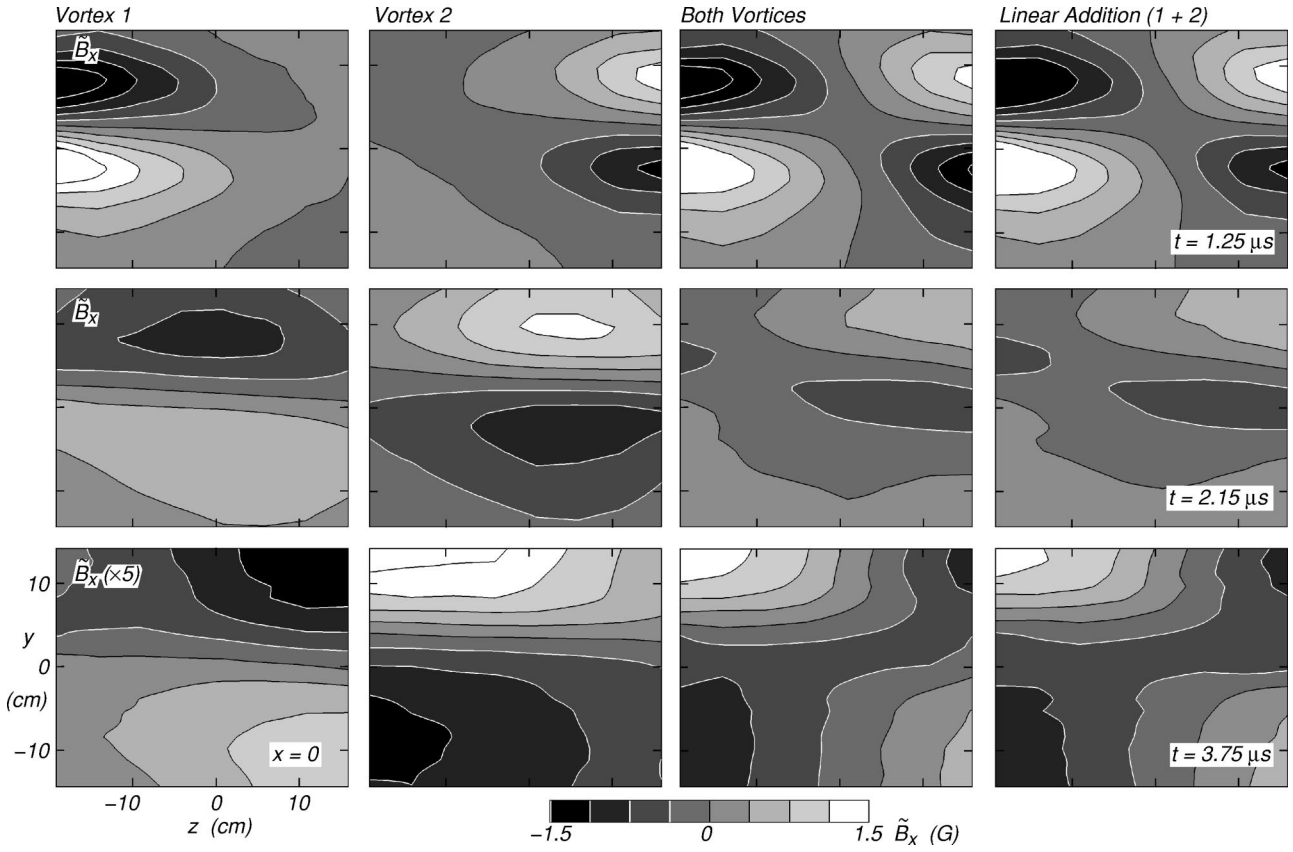

FIG. 5. Toroidal field component $\tilde{B}_\theta = \pm \tilde{B}_x$ in $y-z$ planes ($x=0$) for the head-on collision of two large-amplitude vortices with opposing $\tilde{B}_\theta$ ($B_0=5$ G). Four cases are shown horizontally, i.e., each vortex propagating separately, both together, and a linear superposition of the two individual vortices. Vertically, the data are shown prior to ($t=1.25$ μs), during ($t=2.15$ μs), and after the collision ($t=3.75$ μs). The observations demonstrate that force-free vortices interact linearly.

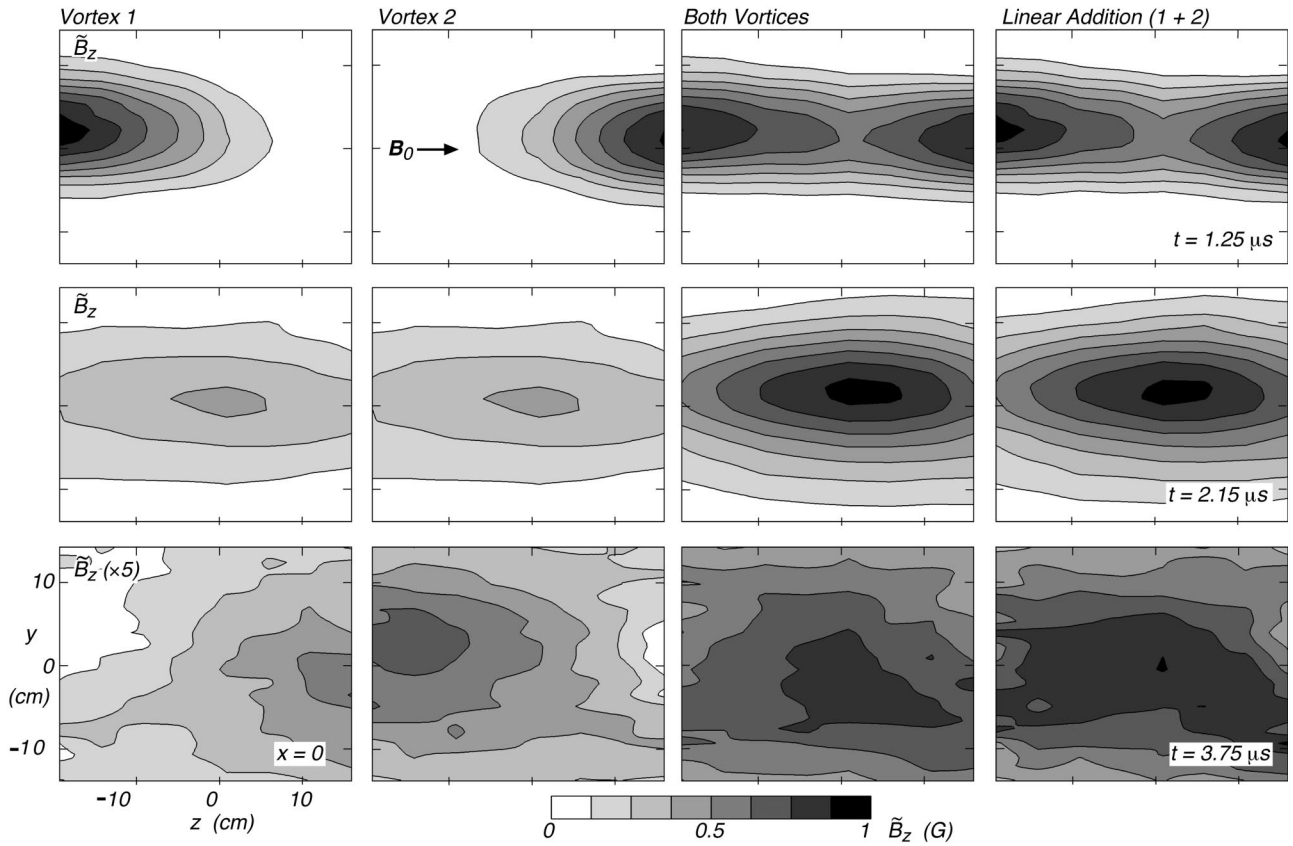

FIG. 6. Poloidal field component $\tilde{B}_z$ in $y-z$ planes ($x=0$) for the head-on collision of two large-amplitude vortices with opposing helicity. As in Fig. 5, four cases are shown horizontally: Each vortex propagating separately, both together, and a linear superposition of the two individual vortices. The data are shown prior to ($t=1.25\ \mu$s), during ($t=2.15\ \mu$s), and after the collision ($t=3.75\ \mu$s) and demonstrate the lack of any nonlinear interactions.

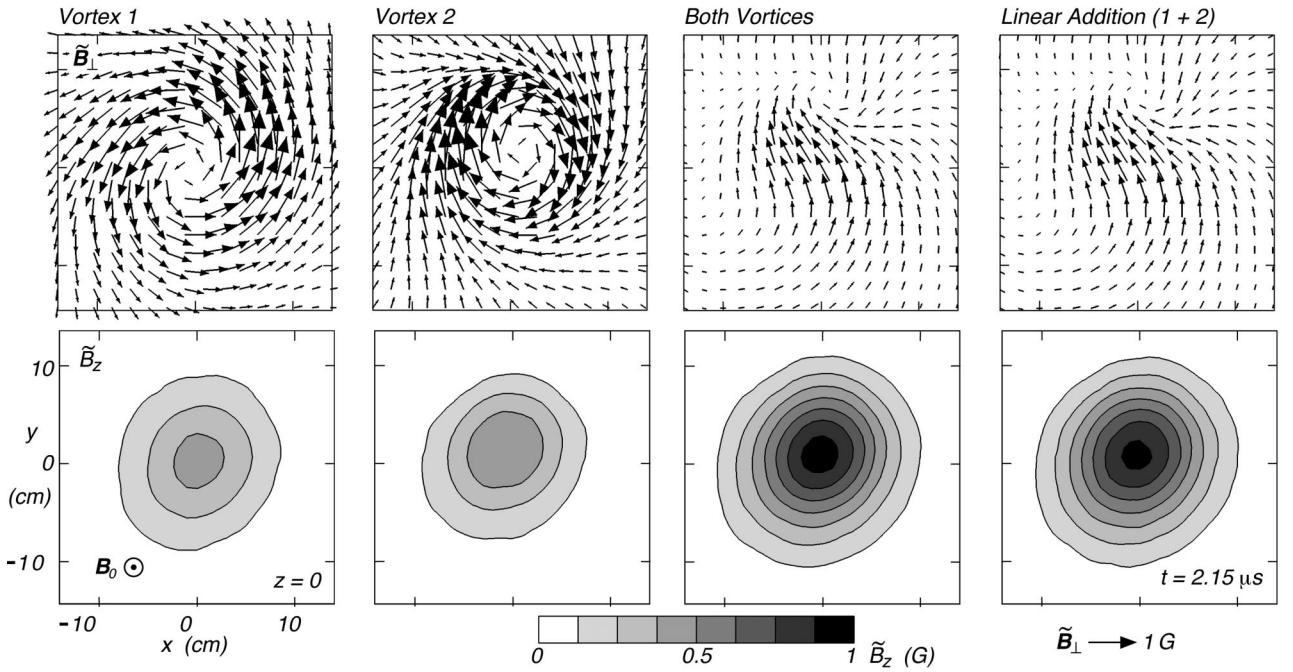

FIG. 7. Field measurements in the transverse $x-y$ plane where the collision occurs ($z=0$). The toroidal fields $\tilde{\mathbf{B}}_\perp \simeq \tilde{\mathbf{B}}_\theta$ are shown as vector fields at the top, the poloidal fields $\tilde{B}_z$ as contour plots at the bottom at the time of collision ($t=2.15\ \mu$s) for the same four cases as in Figs. 5 and 6. During the collision, the poloidal fields $\tilde{B}_z$ of the two vortices add, while the toroidal fields $\tilde{B}_\theta$ nearly cancel, the difference arising from a small offset in the vertical antenna alignment. The interaction is linear and conserves magnetic helicity and energy.

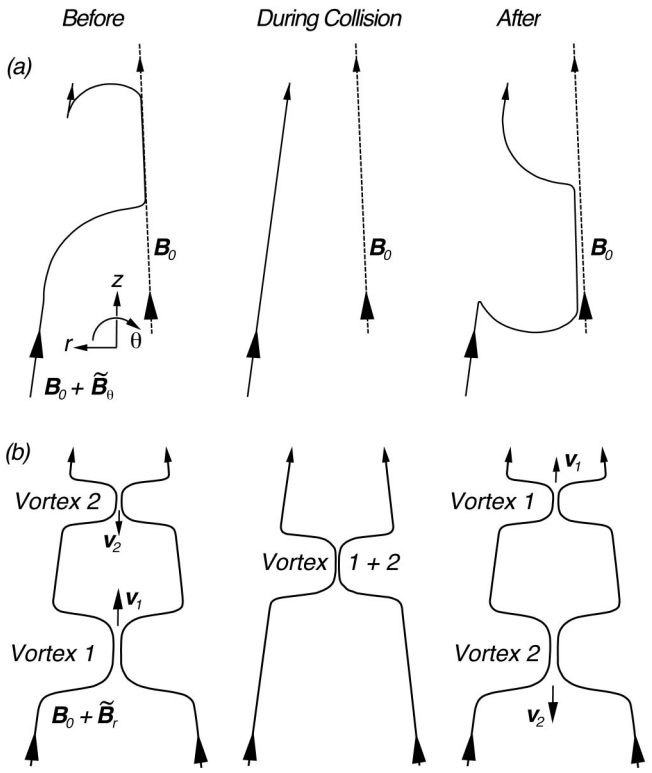

FIG. 8. Schematic pictures of magnetic field lines before, during, and after the head-on collision of two vortices of opposite toroidal and equal poloidal fields. (a) The addition of $\mathbf{B}_0+\tilde{\mathbf{B}}_{\text{tor}}$ creates twisted field lines. (b) The addition of $\mathbf{B}_0+\tilde{\mathbf{B}}_{\text{pol}}$ creates radially bulged field lines. The total field line $\mathbf{B}_0+\tilde{\mathbf{B}}_{\text{tor}}+\tilde{\mathbf{B}}_{\text{pol}}$ is the superposition of both effects.

posing toroidal fields $\pm\tilde{B}_\theta$ of the two vortices. Prior to the collision the field line $\mathbf{B}$ in the upstream section between the two approaching vortices coincides with the unperturbed field $\mathbf{B}_0$ (dashed line), while the field lines downstream of the vortices have been rotated due to the toroidal fluid rotation in of each vortex. During the collision the twist vanishes, although the field line remains rotated from the initial field $\mathbf{B}_0$. The fluid rotation in both vortices is in the same direction before, during, and after the collision. After the collision, the field line between the receding vortices is further rotated by the same angle as the upstream field lines was rotated with respect to $\mathbf{B}_0$. Figure 8(b) shows the constriction of field lines in the region of each vortex, which is due to the identical poloidal fields. Fields and electron fluid flows are consistent with the frozen-in concept: The radial constriction arises from radial inflows and outflows at the front and end of each vortex. The toroidal drift twists the originally straight field line, which requires a toroidal field. Flows and perturbed fields are parallel for the vortex 2 with negative helicity and antiparallel for vortex 1 with positive helicity. Thus, the toroidal flows are the same in each vortex and add during the collision. The added toroidal current produces the enhanced poloidal field. The opposing poloidal drifts of the two vortices cancel during the collision, consistent with the vanishing of the toroidal field. At the moment of collision the toroidal currents form a virtual loop antenna. The subsequent separation of the two vortices can also be viewed as a reradiation of two vortices from a loop antenna. Note that, unlike in MHD, the two parallel toroidal currents (or dipolar magnetic fields) produce no attractive force between the vortices. In EMHD the fields are force-free ($\mathbf{J}\times\tilde{\mathbf{B}}-ne\mathbf{E}=0$) and the vortices pass through each other at a constant velocity.

Although the vortex collision has some aspects of classical reconnection models there are also fundamental differences. In steady-state two-dimensional (2-D) reconnection models,[27] opposing magnetic fields are pushed against each other by opposing fluid flows. The electrodynamics accelerates a charge–neutral fluid whereby magnetic energy is converted into kinetic energy. In the present case the opposing toroidal field components are pushed against each other by wave propagation in opposite directions. The wave velocity is larger and independent of the fluid velocity, which is primarily transverse to the propagation direction. However, as in the physics of reconnection, the toroidal magnetic field energy is lost and the electron fluid is accelerated via Faraday's law. Specifically, the flux change resulting from $\partial\tilde{B}_\theta/\partial t$ produces a radial inductive electric field, which, in EMHD, produces a toroidal $\mathbf{E}_r\times\tilde{\mathbf{B}}_z$ drift along the opposing toroidal field lines. This drift of a charged fluid produces a current and a magnetic field, which in this case enhances the poloidal field. Thus, toroidal magnetic field energy is converted into poloidal field energy and not into kinetic energy of the electrons unless $\beta=nkT_e/(B^2/2\mu_0)\gg 1$, in which case the energy increase is insignificant. The conversion is reversible and occurs when the two vortices re-emerge after the collision.

The observations of vortex collisions with equal toroidal and opposing poloidal fields [Fig. 3(b)] are presented in Fig. 9. A short, small current pulse (500 ns, 12 A) has been applied. For comparison, the left two columns show the fields of one vortex, the right two columns the fields of both vortices excited together. The field components B_θ, B_z are shown as contour plots in the $y-z$ plane at three times during the collision process. During the collision ($t\simeq 0.5\,\mu$s), the poloidal fields cancel and the toroidal fields add, and, as above, energy remains conserved, total self-helicity remains zero, and the positive mutual helicity remains conserved. It is interesting to note that at the center of the midplane ($x=y=z=0$) the vortex field exhibits a 3-D spiral null point,[28] whose spine is along the z axis ($x=y=0$), with the spiral fan in the $x-y$ plane. In the symmetry plane, the plasma current is purely toroidal, forming a virtual loop antenna. Thus, the outgoing vortices may be thought of as being excited by the toroidal current, much in the same way as the wire loop antenna excites the original vortices. This idea has been used to analyze the reflection of a vortex from a conducting boundary: During the approach of the vortex, a toroidal surface current is induced that prevents the penetration of the magnetic field into the conductor ($B_\perp\simeq 0$). The toroidal current reradiates the reflected vortex. However, in contrast to the collision case, magnetic helicity is *not* conserved in the reflection process.[29]

C. Glancing collisions of vortices

A second collision experiment has been performed, where the counterpropagating vortices are offset across $\mathbf{B}_0$ so

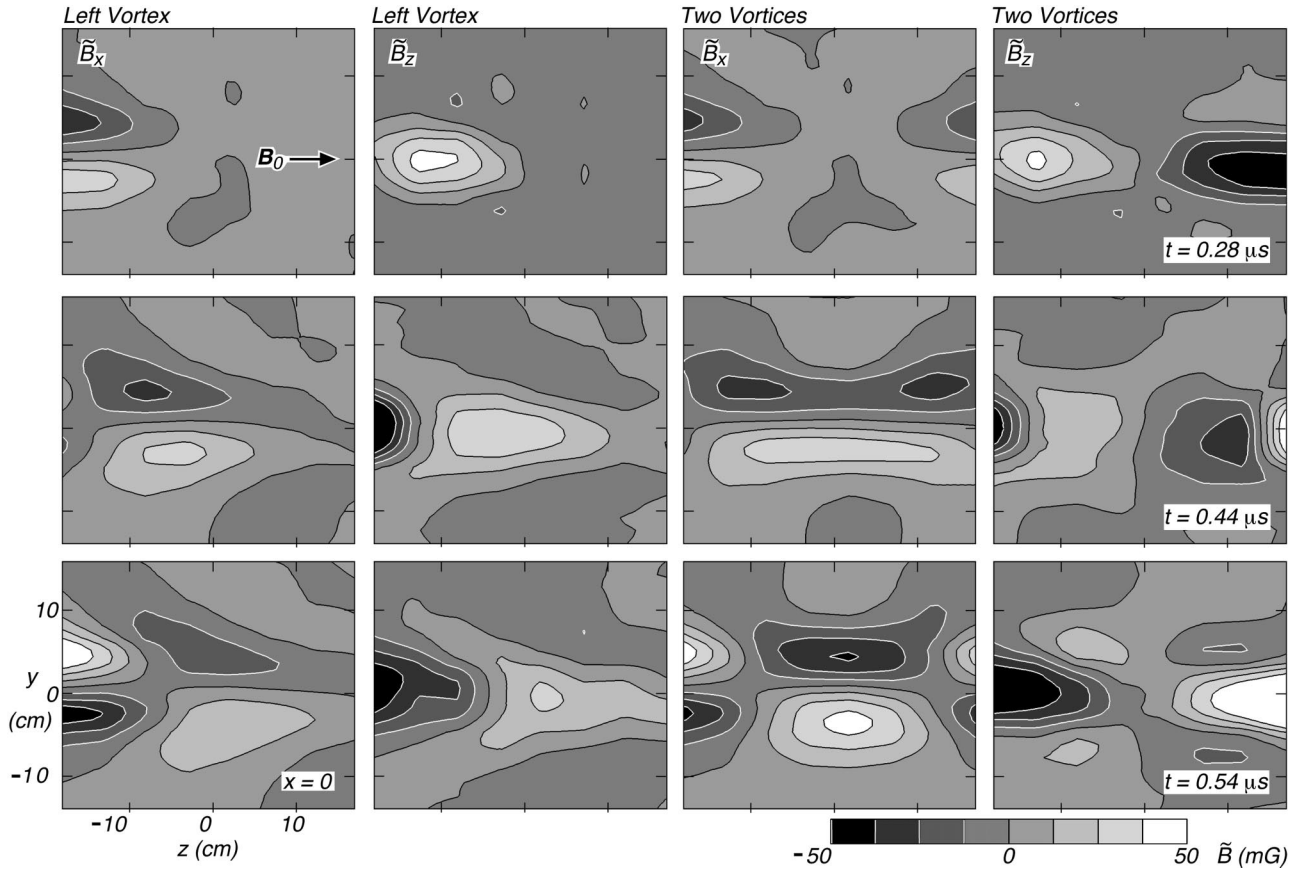

FIG. 9. Vortex collision with opposing poloidal field components $\tilde{B}_z$ and equal toroidal fields $\tilde{B}_\theta$ ($B_0=10$ G). Contour plots show both $\tilde{B}_x$ and $\tilde{B}_z$ in the $y-z$ plane ($x=0$) for a single vortex (left two columns) and both vortices (right two columns) at three different times prior to and during the collision process. The collision produces a solenoidal field B_θ ($\tilde{B}_z \simeq 0$) and is a linear superposition of the fields of two force-free vortices. The initial vortices induced by the turn-on of the antenna currents are followed by vortices of opposite sign induced by the current turn-off.

as to perform a glancing collision. Of particular interest would be a deflection from their original straight paths due to forces and torques between their dipolar fields or merging due to parallel axial currents. Of the two possible configurations we chose vortices with equal toroidal and opposite poloidal fields [Fig. 10(a)]. We first discuss the interaction with the help of schematic field line plots, then show the experimental observations.

The net field lines, $\mathbf{B}=\mathbf{B}_0+\tilde{\mathbf{B}}$, exhibit a left-handed twist in both of the counterpropagating vortices ($\tilde{B}_{\theta,1}<0$, $\tilde{B}_{\theta,2}<0$), which is superimposed on a bulge by vortex 1 ($\tilde{\mathbf{B}}_z \parallel -\mathbf{B}_0$) and a pinch by vortex 2 ($\tilde{\mathbf{B}}_z \parallel \mathbf{B}_0$). Note that vortex 1 has a positive self-helicity, $H_{\rm self}>0$ since $\tilde{B}_\theta<0$, $\tilde{B}_z<0$, but a larger negative mutual helicity ($\tilde{B}_\theta<0$, $B_0>0$), hence its total magnetic helicity is negative as for vortex 2. Figure 10(b) shows, for a model vortex, a set of typical field lines launched from the x-axis in the midplane ($y=z=0$) prior to the vortex collision. The model vortex fields closely resemble the experimental ones but are stronger ($\tilde{B} \leqslant B_0$) so as to clearly show the field line deformation. Prior to the collision, the field line **B** in the upstream section between the two approaching vortices coincides with the unperturbed field $\mathbf{B}_0$. Due to the right-handed fluid rotation in vortex 1 ($v_{\theta,1}>0$, $\tilde{B}_{\theta,1}<0$), the field line well downstream of vortex 1 ($z \ll 0$) has been rotated by an angle θ relative to its unperturbed upstream position. Similarly, field lines downstream of vortex 2 ($z \gg 0$) also experienced a rotation due to $v_{\theta,2}<0$, $\tilde{B}_{\theta,2}<0$. The twists add during the collision, while the bulge and pinch are in juxtaposition. After the collision the field lines between the receding vortices are further rotated relative to the upstream lines.

In order to describe the electrodynamic processes it is helpful to consider only the time-varying vortex fields $\tilde{\mathbf{B}}(B_0=\text{const})$. Figure 11(a) presents selected field lines for the poloidal field components $\tilde{B}_x$, $\tilde{B}_z$ in an $x-z$ plane ($y=0$) as the propagating vortices begin to overlap. On the z axis the opposing field components $\tilde{B}_x$ of the two vortices cancel to form a 2-D X-type null point ($\tilde{B}_x=\tilde{B}_z=0$). As the vortices continue to penetrate one another, the X-type null point merges with the two O-point nulls on axis to form a single island at the origin at the moment of the collision [Fig. 11(b)]. The field topology is that of two antiparallel dipoles in juxtaposition. This field is produced by toroidal currents J_θ, which, at the moment of collision, form two loops that are offset in the x direction by approximately one vortex radius and carry currents in opposite directions.

The poloidal fields are linked by toroidal fields $\tilde{B}_x$, $\tilde{B}_y$, whose field lines are sketched in the central $x-y$ plane (z

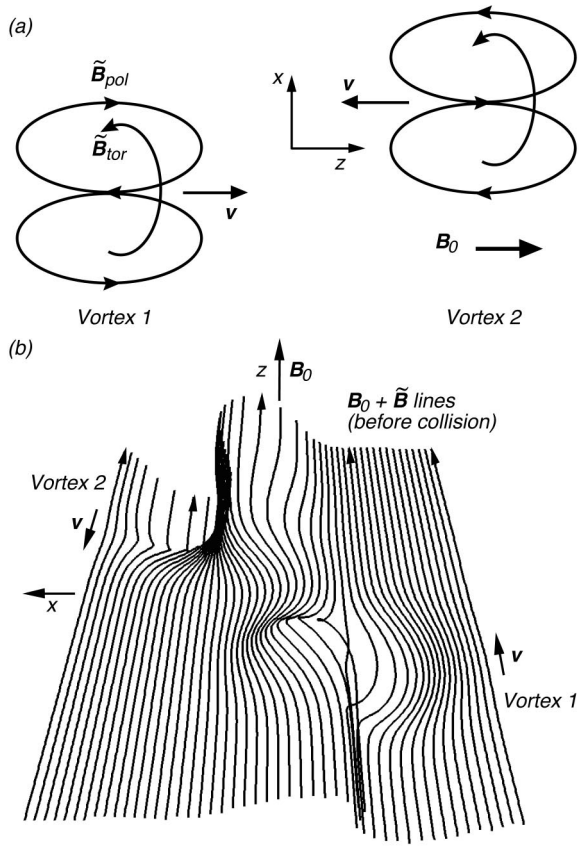

FIG. 10. Schematic figure describing the glancing collision of two counterpropagating vortices. (a) These are radially offset by about one vortex radius, have equal toroidal and opposite poloidal fields, and propagating axially at the whistler velocity **v** along the uniform dc field $\mathbf{B}_0$. (b) Schematic picture of typical lines of the total magnetic field $\mathbf{B}_0+\tilde{\mathbf{B}}$ in the presence of two oppositely propagating vortices. The field lines are launched from the x axis in the midplane ($y=z=0$) and show the twist and pinch/bulge created by the vortices prior to their glancing collision.

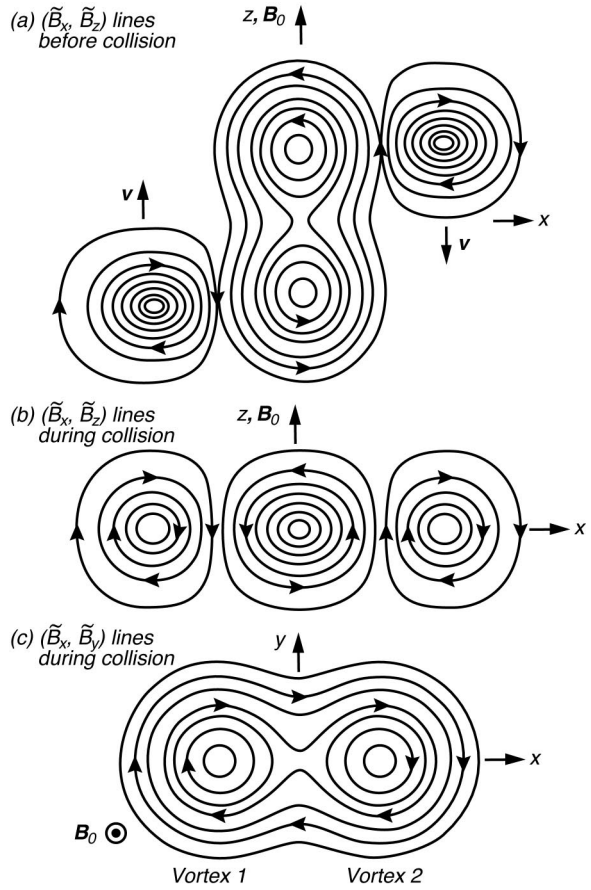

FIG. 11. Schematic picture of typical lines of the vortex magnetic field $\tilde{\mathbf{B}}(\mathbf{r},t)$. (a) Poloidal field lines in plane $y=0$ as the radially offset vortices begin to collide. An X-type null point is formed at the origin. (b) Poloidal field lines at the moment of collision, forming an O-type null point at the origin. (c) Toroidal field lines in the plane $z=0$ at the moment of collision, forming an X-type null point at the origin.

$=0$) at the moment of collision in Fig. 11(c). At the origin, the toroidal field also vanishes such that the vortex field forms a 3-D null point ($\tilde{B}_x=\tilde{B}_y=\tilde{B}_z=0$). The toroidal field is produced by poloidal currents with the same J_z components. At the moment of collision, the poloidal currents form two separate loops closing on the outer side of each vortex, such that $J_x=J_z=0$ on axis. However, the opposing toroidal current loops superimpose at the origin to form a strong current $J_y<0$. This Hall current is driven by an electric field $E_x<0$, which is produced by the toroidal flux change of the propagating vortices. The latter creates loops of inductive electric fields E_x, E_z ($y=0$) whose parallel component E_z is reduced by space-charge fields to values consistent with Ohm's law, which enhances the perpendicular field $E_x<0$ near the origin. The flux change due to the poloidal field $\tilde{B}_z$ of the propagating vortices produces an inductive electric field E_y, which changes sign during the collision. It drives cross-field currents J_x, which connect the poloidal currents of the advancing/receding vortices, but at the moment of collision $E_y=J_x=0$. Thus, poloidal and toroidal fields are coupled via induction and Hall effects. In this glancing collision some poloidal field energy is transferred to toroidal field energy. The transfer would be complete for a head-on collision.

The measured vortex fields and currents during the collision in the mid $x-y$ plane are shown in Fig. 12. Contours of the poloidal field component $\tilde{B}_z$ [Fig. 12(a)] and vector fields of the transverse components $\tilde{\mathbf{B}}_\perp=(\tilde{B}_x,\tilde{B}_y)$ [Fig. 12(b)] show the right-handed field linkage or positive magnetic self-helicity for vortex 1 which propagates along $\mathbf{B}_0$ and negative helicity for the oppositely propagating vortex 2. The axial current density $J_z=(\nabla\times\tilde{\mathbf{B}})_z/\mu_0$ [Fig. 12(c)] has the same sign for both vortices. The transverse current density $\mathbf{J}_\perp=(J_x,J_y)$ [Fig. 12(d)] shows two offset loops of opposite toroidal currents, which are consistent with Ampère's law and the required opposite current helicity density $\mathbf{J}\cdot\tilde{\mathbf{B}}$ in both vortices. Zero net current helicity is conserved during the vortex interaction.

The observed fields are again a linear superposition of those of the individual vortices. Thus, glancing collisions of force-free EMHD vortices produce no interactions between them.

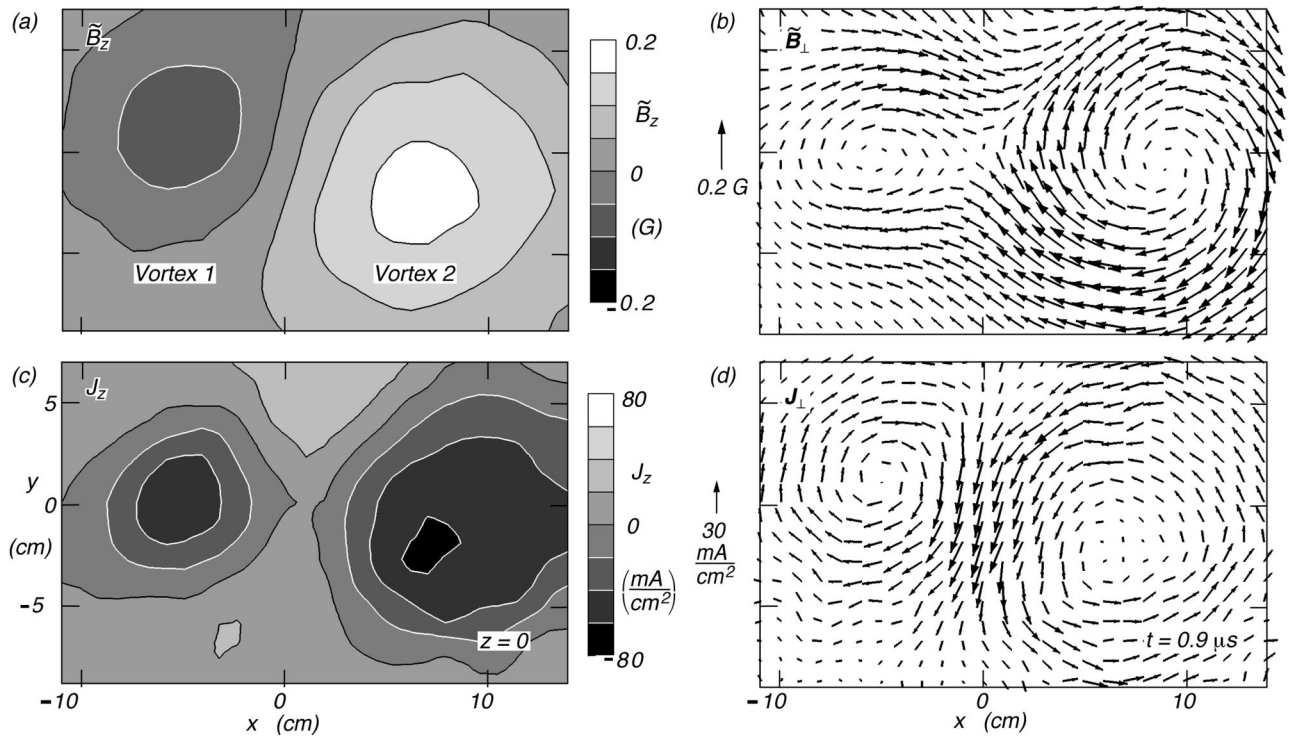

FIG. 12. Observed fields and currents in the $x-y$ plane in the middle between the two antennas ($z=0$) at the moment when two radially offset vortices collide (a) Contours of the axial (poloidal) field component $\tilde{B}_z$. (b) Vector field of the transverse (toroidal) field $\tilde{\mathbf{B}}_\perp$ forming an X-type null point at the center. Vortex 1 with $\mathbf{v} \parallel \mathbf{B}_0$ has right-handed field linkage or positive self-helicity, vortex 2 with $\mathbf{v} \parallel -\mathbf{B}_0$ has negative helicity. (c) Contours of axial (poloidal) current density $J_z=(\nabla\times\tilde{\mathbf{B}})_z/\mu_0$. (d) Field lines of $\mathbf{J}_\perp$, which creates $\tilde{B}_z$, exhibiting a large value $J_y<0$ at the center where $\tilde{B}=0$.

IV. CONCLUSIONS

Experimental observations have shown that EMHD vortices collide without nonlinear interactions. This result may break down when the whistler vortex field exceeds the ambient dc field,[30] but it holds for normalized wave amplitudes, where Alfvén waves or sound waves would interact highly nonlinearly. These results should be of interest in the understanding of whistler turbulence, possibly the inertial range of solar wind fluctuations,[31,32] 3-D EMHD reconnection, vortices in laser–plasma interactions,[33] and rf heating with whistlers.

ACKNOWLEDGMENT

The authors gratefully acknowledge support for this work from National Science Foundation Grant No. PHY 9713240.

[1]A. S. Kingsep, K. V. Chukbar, and V. V. Yan'kov, in *Reviews of Plasma Physics*, edited by B. Kadomtsev (Consultants Bureau, New York, 1990), Vol. 16, p. 243.
[2]S. V. Bulanov, F. Pegoraro, and A. S. Sakharov, Phys. Fluids B **4**, 2499 (1992).
[3]J. F. Drake, R. G. Kleva, and M. E. Mandt, Phys. Rev. Lett. **73**, 1251 (1994).
[4]M. L. Goldstein, D. A. Roberts, and C. A. Fitch, J. Geophys. Res. **99**, 11 519 (1994).
[5]R. J. Leamon, C. W. Smith, N. F. Ness, W. H. Matthaeus, and H. K. Wong, J. Geophys. Res. **103**, 4775 (1998).
[6]F. F. Chen and R. W. Boswell, IEEE Trans. Plasma Sci. **25**, 1245 (1997).
[7]B. V. Weber, R. J. Commisso, P. J. Goodrich, J. M. Grossmann, D. D. Hinshelwood, P. F. Ottinger, and S. B. Swanekamp, Phys. Plasmas **2**, 3893 (1995).
[8]I. R. Jones, C. Deng, I. M. El-Fayoumi, and P. Euripides, Phys. Rev. Lett. **81**, 2072 (1998).
[9]J. M. Urrutia, R. L. Stenzel, and C. L. Rousculp, Phys. Plasmas **2**, 1100 (1995).
[10]R. L. Stenzel, J. M. Urrutia, and C. L. Rousculp, Phys. Plasmas **2**, 1114 (1995).
[11]M. B. Isichenko and A. M. Marnachev, Sov. Phys. JETP **66**, 702 (1987).
[12]J. M. Urrutia and R. L. Stenzel, Phys. Plasmas **3**, 2589 (1996).
[13]R. L. Stenzel, J. M. Urrutia, and M. C. Griskey, in *Magnetic Helicity in Space and Laboratory Plasmas*, Geophysics Monograph, edited by M. Brown, R. Canfield, and A. Pevtsov (American Geophysical Union, Washington, DC, 1999) Vol. 111, pp. 179–186.
[14]O. U. V. Fuentes and J. F. Van Heijst, Phys. Fluids **7**, 2735 (1995).
[15]C. F. Driscoll and K. S. Fine, Phys. Fluids B **2**, 1359 (1990).
[16]M. Makino, T. Kamimura, and T. Taniuti, J. Phys. Soc. Jpn. **50**, 980 (1981).
[17]S. Oughton, W. H. Matthaeus, and S. Ghosh, Phys. Plasmas **5**, 4235 (1998).
[18]W. H. Bostick, IEEE Trans. Plasma Sci. **17**, 69 (1989).
[19]R. L. Stenzel and W. F. Daley, United States Patent No. 4,216,405, August 5, 1980.
[20]H. K. Moffatt and D. W. Moore, J. Fluid Mech. **87**, 749 (1979).
[21]T. J. Dolan, *Fusion Research*, (Pergamon, New York, 1982), Vol. 2, p. 329.
[22]C. L. Rousculp, R. L. Stenzel, and J. M. Urrutia, Phys. Plasmas **2**, 4083 (1995).
[23]R. L. Stenzel, J. M. Urrutia, and C. L. Rousculp, Phys. Fluids B **5**, 325 (1993).
[24]P. A. Folkes, H. Ikezi, and R. Davis, Phys. Rev. Lett. **45**, 902 (1980).
[25]Y. Nakamura, J. Plasma Phys. **38**, 461 (1987).
[26]K. E. Lonngren, Opt. Quantum Electron. **30**, 615 (1998).
[27]V. M. Vasyliunas, Rev. Geophys. Space Phys. **13**, 303 (1975).
[28]C. E. Parnell, J. M. Smith, T. Neukirch, and E. R. Priest, Phys. Plasmas **3**, 759 (1996).

[29]R. L. Stenzel, J. M. Urrutia, and M. C. Griskey, Phys. Rev. Lett. **82**, 4006 (1999).
[30]R. L. Stenzel and J. M. Urrutia, Phys. Rev. Lett. **81**, 2064 (1998).
[31]P. Goldreich and S. Sridhar, Astrophys. J. **485**, 680 (1997).
[32]F. Pegoraro, B. N. Kuvshinov, J. Rem, and T. J. Schep, Adv. Space Res. **19**, 1823 (1997).
[33]S. V. Bulanov, M. Lontano, T. Zh. Esirkepov, F. Pegoraro, and A. M. Pukhov, Phys. Rev. Lett. **76**, 3562 (1996).